Semiclassical two-step model for strong-field ionization

N. I. Shvetsov-Shilovski,[1,*] M. Lein,[1] L. B. Madsen,[2] E. Räsänen,[3] C. Lemell,[4]
J. Burgdörfer,[4,5] D. G. Arbó,[6] and K. Tőkési[5,7]

[1]*Institut für Theoretische Physik and Centre for Quantum Engineering and Space-Time Research, Leibniz Universität Hannover, D-30167 Hannover, Germany*
[2]*Department of Physics and Astronomy, Aarhus University, 8000 Århus C, Denmark*
[3]*Department of Physics, Tampere University of Technology, FI-33101 Tampere, Finland*
[4]*Institute for Theoretical Physics, Vienna University of Technology, A-1040 Vienna, Austria, European Union*
[5]*Institute for Nuclear Research, Hungarian Academy of Sciences, H-4001 Debrecen, Hungary, European Union*
[6]*Institute for Astronomy and Space Physics, IAFE (UBA-Conicet), Buenos Aires, Argentina*
[7]*ELI-HU Nonprofit Ltd., Dugonics tér 13, 6720 Szeged, Hungary*

(Received 18 April 2016; published 19 July 2016)

We present a semiclassical two-step model for strong-field ionization that accounts for path interferences of tunnel-ionized electrons in the ionic potential beyond perturbation theory. Within the framework of a classical trajectory Monte Carlo representation of the phase-space dynamics, the model employs the semiclassical approximation to the phase of the full quantum propagator in the exit channel. By comparison with the exact numerical solution of the time-dependent Schrödinger equation for strong-field ionization of hydrogen, we show that for suitable choices of the momentum distribution after the first tunneling step, the model yields good quantitative agreement with the full quantum simulation. The two-dimensional photoelectron momentum distributions, the energy spectra, and the angular distributions are found to be in good agreement with the corresponding quantum results. Specifically, the model quantitatively reproduces the fanlike interference patterns in the low-energy part of the two-dimensional momentum distributions, as well as the modulations in the photoelectron angular distributions.

DOI: 10.1103/PhysRevA.94.013415

I. INTRODUCTION

Strong-field physics is concerned with highly nonlinear phenomena originating from the interaction of strong laser radiation with atoms and molecules. Above-threshold ionization (ATI), high-order harmonic generation, and nonsequential double ionization are the most well-known examples (see Refs. [1–5] for reviews). Among the main theoretical approaches used to understand these diverse phenomena are the direct numerical solution of the time-dependent Schrödinger equation (TDSE), the strong-field approximation (SFA) [6–8], and semiclassical models applying a classical description of an electron after it has been released from an atom, e.g., by tunneling ionization [9–11]. The most widely known examples of semiclassical approaches are the two-step model for ionization [12–14] and the three-step models for harmonic radiation and rescattering [15,16]. In the first step of the two-step model an electron tunnels out of an atom, and in the second step it propagates in the laser field. The third step involves the rescattering of the returning electron with the residual ion. Thus, the three-step model allows for a qualitative description of rescattering-induced processes: high-order ATI, high-order harmonic generation, and nonsequential double ionization.

Although significant progress has been made over the last two decades in development of the theoretical approaches based on the SFA and, particularly, on the TDSE (see, e.g., Refs. [17,18] and references therein), the semiclassical models are still extensively used in strong-field physics. The reason is that these models have a number of advantages. Indeed, semiclassical simulations can help to identify the specific mechanisms responsible for the phenomena under consideration and provide an illustrative picture in terms of classical trajectories. For example, the three-step model explained the cutoffs in high-order harmonic generation [19,20] and high-order ATI spectra [21], the maximum angles in the photoelectron angular distributions [22], and the characteristic momenta of recoil ions of the nonsequential double ionization [23,24].

In their original formulation, the two-step and three-step models do not take into account the effect of the Coulomb potential of the parent ion on the electron motion after ionization. The inclusion of the Coulomb potential into the two-step model made it possible to reveal the so-called Coulomb focusing effect [25]. Employing classical trajectory Monte Carlo (CTMC) simulations for the second step, the Coulomb cusp in the angular distribution of strong-field ionized electrons could be identified [26]. Among the more recent examples of application of the semiclassical models with the Coulomb potential are the investigation of the so-called "ionization surprise" [27], i.e., the low-energy structures in strong-field ionization by midinfrared pulses [28–36], the study of the angular shifts of the photoelectron momentum distributions in close to circularly polarized laser fields [37–39], and the analysis of the nonadiabatic effects in strong-field ionization (see, e.g., Refs. [40–42]). Semiclassical simulations are often (but not necessarily always) computationally much simpler than the direct numerical solution of the TDSE. Sometimes rather large ensembles of classical trajectories are needed (e.g., in the present case about 10^9 trajectories) in order to get statistically reliable results or resolve fine details of the photoelectron differential distributions. Nevertheless,

*n79@narod.ru

semiclassical models remain powerful tools even in this situation, since trajectory-based simulations can be easily and very efficiently parallelized even on modest computer clusters. Moreover, there are still many strong-field problems, for which semiclassical models are the only feasible approach. Well-known examples of the latter category include the nonsequential double ionization of atoms by elliptically [43–45] and circularly [46] polarized fields as well as the nonsequential double ionization of molecules [47]. Therefore, improvements of the semiclassical models of strong-field phenomena are being sought with the goal to render them quantitatively predictive.

Recently, some progress among these lines has been achieved. For example, a criterion of applicability of the two-step model with the Coulomb potential of the parent ion was formulated in Ref. [48]. Within a purely classical treatment of the electron dynamics subsequent to tunnel ionization, interference structures in the photoelectron spectrum and two-dimensional momentum distribution [49–52] cannot be reproduced. This deficiency has been overcome by a semiclassical model denoted by the authors of [53] as the "quantum trajectory Monte Carlo (QTMC)."[1] This model makes it possible to include interference effects into the two-step model with the Coulomb potential. Accordingly, each classical trajectory is associated with a phase determined by the classical action, and the contributions of all trajectories leading to a given final momentum calculated by a CTMC approach are added coherently. The QTMC model has already been used in the study of nonadiabatic effects in tunneling ionization of atoms in elliptically polarized laser fields [42]. A similar approach, but disregarding the Coulomb potential, was used in Ref. [55] to investigate the holographic interference patterns in strong-field ionization of N_2, O_2, and CO_2. Very recently, the QTMC model has been applied to the identification of resonance structures in the low-energy part of the photoelectron spectra [56] and to the study of the nonadiabatic subcycle electron dynamics in orthogonally polarized two-color laser fields [57].

The Coulomb-corrected strong-field approximation (CCSFA) [30,58,59] has been applied to analyze results of experiment and theory. The CCSFA invokes first-order perturbation theory [60] to include the Coulomb potential. Likewise, according to the Supplemental Material in Ref. [53], the QTMC model includes the Coulomb effect in a perturbative manner, a point that we discuss below. It is, therefore, of interest to formulate a semiclassical two-step (SCTS) model that accounts for the Coulomb potential beyond the semiclassical perturbation theory. Our present approach is based on the theory of semiclassical time-dependent propagators (see, e.g., Refs. [61,62] for a textbook treatment). Here we derive a semiclassical expression for the transition amplitude for strong-field ionization that differs from the one used in the QTMC and CCSFA models improving the agreement with full quantum simulations.

The paper is organized as follows. In Sec. II we briefly review previous two-step models that invoke semiclassical approximations at various stages of their development. In Sec. III we present our semiclassical two-step model that combines the CTMC method for trajectory sampling with the phase of the semiclassical propagator and discuss its numerical implementation. The application to the benchmark case of strong-field ionization of atomic hydrogen and the comparison with TDSE results are presented in Sec. IV, followed by concluding remarks in Sec. V. Atomic units are used throughout the paper unless indicated otherwise.

II. TWO-STEP MODELS

The two-step models for direct strong-field ionization as well as their three-step extensions typically invoke semiclassical approximations to the full quantum dynamics at various levels. We briefly sketch the major steps involved in order to delineate the point of departure of the present SCTS model. It should be stressed that our model is different from SFA-type models such as the CCSFA model [30,58,59] as the latter are applicable for arbitrary values of the Keldysh parameter $\gamma = \omega\kappa/F$ [6] (here ω is the angular frequency of the laser field, F is the field amplitude, and $\kappa = \sqrt{2I_p}$, where I_p is the ionization potential). In contrast to this, we employ instantaneous tunneling ionization rates. The description of the ionization step by tunneling is expected to be accurate only for small values of the Keldysh parameter, $\gamma \ll 1$.

The starting point of the semiclassical approximation is the assumption that the (classical) action in the Feynman propagator is asymptotically large compared to the quantum action $\hbar$ such that the path integral over (in general, nonclassical) paths can be performed by the saddle-point approximation. Equivalently, the semiclassical approximation can be viewed as the leading term in an $\hbar^n$ expansion as $\hbar \to 0$. Accordingly, the expression for the matrix element of the semiclassical propagator U_{SC} between the initial state at time t_1 and the final state at time $t_2 (t_2 > t_1)$ reads [63–65] (see Refs. [61] and [62] for a textbook treatment)

$$\langle \vec{r}_2|U_{\rm SC}(t_2,t_1)|\vec{r}_1\rangle = \left[-\frac{\det(\partial^2\phi_1(\vec{r}_1,\vec{r}_2)/\partial\vec{r}_1\partial\vec{r}_2)}{(2\pi i)^3}\right]^{1/2} \times \exp[i\phi_1(\vec{r}_1,\vec{r}_2)]. \quad (1)$$

Here $\vec{r}_1$ and $\vec{r}_2$ are the spatial coordinates of a particle at times t_1 and t_2, respectively, and the phase $\phi_1(\vec{r}_1,\vec{r}_2) = S_1(\vec{r}_1,\vec{r}_2)/\hbar$ is given in terms of the action S_1,

$$S_1(\vec{r}_1,\vec{r}_2) = \int_{t_1}^{t_2} \{\vec{p}(t)\dot{\vec{r}}(t) - H[\vec{r}(t),\vec{p}(t)]\}dt, \quad (2)$$

where, in turn, $H[\vec{r}(t),\vec{p}(t)]$ is the classical Hamiltonian function as a function of the canonical coordinates $\vec{r}(t)$ and momenta $\vec{p}(t)$. In dipole approximation the Hamiltonian function of an electron moving in laser and Coulomb fields is

[1]This model should not be confused with another approach termed quantum trajectory Monte Carlo that was used for the solution of the Liouville equation for open quantum systems [54]. It is based on an ensemble of solutions of a stochastic Schrödinger equation, each of which corresponds to a quantum trajectory in Hilbert space.

given by

$$H[\vec{r}(t),\vec{p}(t)] = \frac{p^2(t)}{2} + \vec{F}(t)\cdot\vec{r}(t) - \frac{Z}{r(t)}, \tag{3}$$

where $\vec{F}(t)$ is the electric field and Z is the ionic charge. The prefactor in Eq. (1) contains the determinant of $-\partial^2 S_1/\partial\vec{r}_1\partial\vec{r}_2$, frequently referred to as the van Vleck (vV) determinant for multidimensional systems, which is independent of $\hbar$. The phase factor $\exp(i\phi_i)$ is nonanalytic as $\hbar \to 0$ and accounts for the nonuniform approach to the classical limit via increasingly fast oscillations (see Ref. [66]).

For classically allowed processes, the vV-determinant governs the classical phase-space density (or probability density) for the phase flow from $\vec{r}_1$ to $\vec{r}_2$ within the time interval $t_2 - t_1$. Higher-order corrections in $\hbar$ are neglected in Eq. (1) from the outset. Using atomic units in the following we do not display the $\hbar$ dependence explicitly but, instead, express the semiclassical limit in terms of the de Broglie wavelength λ_{dB} exploiting the equivalence of vanishing de Broglie wavelength $\lambda_{dB} \to 0$ and the limit $\hbar \to 0$.

The point to be emphasized is that the applicability of the saddle-point approximation, and, in turn, the semiclassical limit for the ionization process in the presence of laser and Coulomb fields is, *a priori*, not obvious. The tunneling process is intrinsically nonclassical and the de Broglie wavelength $\lambda_{dB}(E)$ of slow electrons close to the tunneling exit is, in general, not small compared to the exit coordinate η or the width of the barrier; i.e., the semiclassical relation $\lambda_{dB} \ll \eta$ is violated.

A. Semiclassical approximation for the first step

The starting point for the first step of strong-field ionization, the tunneling through the barrier formed by the atomic (ionic) potential and the interaction with the electromagnetic field, is the quantum transition matrix element in distorted-wave Born approximation (SFA)

$$M_{\rm SFA}(\vec{k}) = -i\int_{-\infty}^{\infty} dt\,\langle\psi_{\vec{k}}(t)|V_L(t)|\psi_i(t)\rangle, \tag{4}$$

where $|\psi_i(t)\rangle$ is the bound initial state and $|\psi_{\vec{k}}(t)\rangle$ is the Volkov state after tunneling with the asymptotic momentum $\vec{k}$,

$$\psi_{\vec{k}}(\vec{r},t) = \exp\left\{i[\vec{k}+\vec{A}(t)/c]\vec{r} - \frac{i}{2}\int_{-\infty}^{t} dt'[\vec{k}+\vec{A}(t')/c]^2\right\}. \tag{5}$$

Equation (4) is referred to as the strong-field approximation as in the final state the ionic potential is considered to be negligible in comparison to the interaction $V_L(t) = \vec{F}(t)\cdot\vec{r}$. Note that we use a length gauge in Eqs. (4) and (5) and define the strong electric field $\vec{F}(t) = -\frac{1}{c}\frac{d\vec{A}}{dt}$ through the vector potential $\vec{A}(t)$. The time integral is evaluated within the framework of the saddle-point approximation assuming that the effective phase (or action)

$$S(\vec{k},t) = \int_{-\infty}^{t} dt'\left\{\frac{1}{2}[\vec{k}+\vec{A}(t')/c]^2 - \varepsilon_i\right\} \tag{6}$$

is large and rapidly varying with t, thereby invoking the semiclassical (SC) limit. The prerequisites for the applicability of this semiclassical limit are the ponderomotive energy U_p and the ionization potential $I_p = -\varepsilon_i$ to be large compared to the photon energy ω, $U_p/\omega \gg 1$ and $I_p/\omega \gg 1$. Unlike Eq. (1), the semiclassical approximation is applied to the transition matrix element [Eq. (4)] rather than to the propagator. Accordingly (see, e.g., [67,68]),

$$M_{\rm SFA}^{\rm SC} = \sum_j \frac{\exp\left[iS\left(\vec{k},t_s^j\right)\right]}{\left[\frac{\partial^2}{\partial t^2}S\left(\vec{k},t_s^j\right)\right]^{1/2}} V_{\vec{k}}^j, \tag{7}$$

with $V_{\vec{k}}^j$ containing the spatial dependencies of the transition matrix element. The saddle-point equation

$$\frac{\partial}{\partial t}S(\vec{k},t_s) = \frac{1}{2}[\vec{k}+\vec{A}(t_s)/c]^2 + I_p = 0 \tag{8}$$

has complex solutions in t, $t_s^j = t_0^j + it_t^j$, where the real part t_0 is referred to as the ionization time and the imaginary part t_t as the tunneling time. Because of the complex solutions, the emerging trajectories are often referred to as quantum trajectories; see Refs. [67,69]. When more than one saddle point contributes ($j = 1,\ldots$), Eq. (7) can give rise to semiclassical path interferences.

Frequently employed approximate evaluations of Eq. (7) include the Perelomov-Popov-Terent'ev or Ammosov-Delone-Krainov rates for adiabatic tunneling in which t_0 coincides with the extremum of the electric field F [9–11]:

$$w(t_0,v_{0,\perp}) \sim \left|M_{\rm SFA}^{\rm SC}\right|^2 \sim \exp\left[-\frac{2\kappa^3}{3F(t_0)}\right]\exp\left[-\frac{\kappa v_{0,\perp}^2}{F(t_0)}\right]. \tag{9}$$

For simplicity, we omit the preexponential factor in Eq. (9). Although this factor changes the total ionization rate by several orders of magnitude, for atoms it only slightly affects the shape of the photoelecton momentum distributions. When applying Eq. (9), a simple and frequently used choice is that the electron emerges with vanishing velocity component along the laser polarization direction $v_{0,z} = 0$, while $v_{0,\perp}$ is Gaussian distributed. It is common to apply Eq. (9) as a quasistatic rate [70], i.e., for tunneling ionization for laser phases other than the field extremum, with $F(t_0)$ in Eq. (9) denoting the instantaneous field. Nonzero longitudinal velocity components $v_{0,z} \neq 0$ appear near the tunnel exit when the subbarrier motion is modeled by the strong-field approximation [71].

The coordinates of the tunneling exit can be conveniently determined by using the fact that for an electron in a time-independent electric field F and the Coulomb potential, $-Z/r$, both the classical Hamilton-Jacobi equation [72] and the stationary Schrödinger equation are separable in parabolic coordinates (see Refs. [9,73])

$$\xi = r + z, \quad \eta = r - z, \quad \phi = \arctan\left(\frac{y}{x}\right). \tag{10}$$

If the electric field points along the positive z direction, the electron is trapped by an attractive potential along the ξ coordinate and can tunnel out only in the η direction. The

tunnel exit coordinate η is then obtained from the equation

$$-\frac{\beta_2(F)}{2\eta}+\frac{m^2-1}{8\eta^2}-\frac{F\eta}{8}=-\frac{I_p(F)}{4}, \tag{11}$$

where

$$\beta_2(F)=Z-(1+|m|)\frac{\sqrt{2I_p(F)}}{2} \tag{12}$$

is the separation constant (see, e.g., Ref. [74]) and m is the magnetic quantum number of the initial state. In Eq. (12) we have allowed for the Stark shift of the initial state, i.e., of the ionization potential,

$$I_p(F)=I_p+\tfrac{1}{2}(\alpha_N-\alpha_I)F^2, \tag{13}$$

where F is the instantaneous field amplitude at the ionization time t_0 and α_N and α_I are the static polarizabilities of an atom and of its ion, respectively [75]. With Eqs. (11) and (9), the initial conditions for the propagation of trajectories subsequent to tunneling ionization, i.e., for the second step, are determined.

As the focus of the present work is the improved semiclassical description of the second step, we treat in the following the output of the first step, in particular the initial velocity (or momentum) distribution at the tunneling exit [see, e.g., Eq. (9)] as adjustable input. We use two different initial phase-space distributions resulting from the tunneling step as initial conditions for the post-tunneling semiclassical propagation. Both choices of distributions are described by Eq. (9). The difference is that in one case, the initial parallel velocity $v_{0,z}$ is set to zero, whereas in the other case, it is set to a nonzero value predicted by the SFA [71].

B. Semiclassical approximation for the second step

The position and momentum distributions at the tunneling exit serve as initial conditions for the propagation of classical trajectories in the second step. In the simplest approximation, the quiver motion for a selected set of trajectories for free electrons in the electromagnetic field is treated, thereby neglecting the atomic force field [14–16,20]. More advanced descriptions employ full CTMC simulations treating the laser field and the atomic force field on equal footing by solving Newton's equation of motion,

$$\frac{d^2\vec{r}(t)}{dt^2}=-\vec{F}(t)-\frac{Z\vec{r}(t)}{r^3(t)}, \tag{14}$$

for a large number of initial conditions (typically $\geqslant 10^7$), thereby sampling the initial phase-space distribution after tunneling [26].

For the propagation of the electron in the combined fields [Eq. (14)], a semiclassical approximation in terms of a coherent superposition of amplitudes appears justified since classical-quantum correspondence holds separately for both the propagation in the Coulomb field and in the laser field. For the linear potential of a charged particle in the external field, $V_L=\vec{F}\cdot\vec{r}$, the Ehrenfest theorem holds for Newton's law, $\langle\vec{\nabla}V_L\rangle=\vec{\nabla}V_L(\langle\vec{r}\rangle)$. For the long-range Coulomb potential $\lambda_{dB}(E)$ is negligible compared to the infinite range of the potential at any energy E. However, an extension of CTMC simulations to the semiclassical domain faces considerable difficulties in view of the intrinsic numerical instability, which is closely related to the nonuniform convergence to the classical limit mentioned above. Superposition of a large number of amplitudes associated with trajectories with rapidly oscillating phases fails to yield converged scattering amplitudes in the asymptotic limit $t\to\infty$ [66]. One key ingredient is therefore the binning of the trajectories according to the appropriate final canonical momenta and restricting coherent superpositions to those trajectories within each bin. For bound-state excitation driven by ultrashort pulses this corresponds to binning of the action variable, i.e., to a quantization of classical trajectories. This quantized classical trajectory Monte Carlo method [76] can accurately account for quantum revivals and dephasing in Rydberg manifolds.

For strong-field ionization, the final states lie in the continuum and are binned according to their momenta in cells in momentum space [42,57], $[k_i,k_i+\Delta k_i]$, with $i=x,y,z$. Accordingly, the amplitudes associated with all n_p trajectories taking off at t_0^j with initial velocity $\vec{v}_0^{\,j}$ $(j=1,\ldots,n_p)$ reaching the same bin centered at $\vec{k}=(k_x,k_y,k_z)$ are added coherently. Thus, the ionization probability $R(\vec{k})$ for this final momentum $\vec{k}$ is given by

$$R(\vec{k})=\left|\sum_{j=1}^{n_p}\sqrt{w\left(t_0^j,\vec{v}_0^{\,j}\right)}\exp\left[i\Phi\left(t_0^j,\vec{v}_0^{\,j}\right)\right]\right|^2, \tag{15}$$

where $w(t_0^j,v_0^j)$ is the probability density of the initial conditions. The sum over j samples the classical phase flow from $\vec{v}_0$ to the bin $\vec{k}$ corresponding to the vV determinant as determined by CTMC. $\Phi(t_0^j,\vec{v}_0^{\,j})$ is the phase that each trajectory carries. When the interference phases of trajectories reaching the same bin are neglected, the classical CTMC probability density

$$R(\vec{k})=\sum_{j=1}^{n_p}w\left(t_0^j,\vec{v}_0^{\,j}\right) \tag{16}$$

emerges. In the QTMC model [53], the phase in Eq. (15) was approximated by

$$\Phi^{\mathrm{QTMC}}\left(t_0^j,\vec{v}_0^{\,j}\right)\approx I_p t_0^j-\int_{t_0^j}^{\infty}\left[\frac{p^2(t)}{2}-\frac{Z}{r(t)}\right]dt. \tag{17}$$

We relate the phase in Eq. (17) to our semiclassical phase in Sec. III A.

III. FORMULATION OF THE MODEL

A. Semiclassical expression for the phase

The two key ingredients of the present semiclassical two-step model are the choice of an initial momentum distribution emerging from the first tunneling step based on SFA estimates and a proper semiclassical description for the second step. This approach accounts for the expectation that the semiclassical limit is applicable for the evolution of the liberated electron in the combined laser and ionic force fields. We describe the second step of the two-step model using the expression for the matrix element of the semiclassical propagator U_{SC}.

In addition to its coordinate representation [Eq. (1)], three equivalent forms involving different combinations of phase-space coordinates exist [63,77]:

$$\langle \vec{r}_2|U_{\rm SC}(t_2,t_1)|\vec{p}_1\rangle = \left[-\frac{\det(\partial^2\phi_2(\vec{p}_1,\vec{r}_2)/\partial\vec{p}_1\partial\vec{r}_2)}{(2\pi i)^3}\right]^{1/2} \times \exp[i\phi_2(\vec{p}_1,\vec{r}_2)], \tag{18a}$$

$$\langle \vec{p}_2|U_{\rm SC}(t_2,t_1)|\vec{r}_1\rangle = \left[-\frac{\det(\partial^2\phi_3(\vec{r}_1,\vec{p}_2)/\partial\vec{r}_1\partial\vec{p}_2)}{(2\pi i)^3}\right]^{1/2} \times \exp[i\phi_3(\vec{r}_1,\vec{p}_2)], \tag{18b}$$

$$\langle \vec{p}_2|U_{\rm SC}(t_2,t_1)|\vec{p}_1\rangle = \left[-\frac{\det(\partial^2\phi_4(\vec{p}_1,\vec{p}_2)/\partial\vec{p}_1\partial\vec{p}_2)}{(2\pi i)^3}\right]^{1/2} \times \exp[i\phi_4(\vec{p}_1,\vec{p}_2)]. \tag{18c}$$

They describe the propagation from the initial position ($\vec{r}_1$) or momentum coordinate ($\vec{p}_1$) to a final position ($\vec{r}_2$) or momentum coordinate ($\vec{p}_2$) within the time interval $t_2 - t_1$. The phases ϕ_i, $i = 2,3,4$ in Eqs. (18a)–(18c) are given by the classical action associated with the corresponding canonical transformations,

$$\phi_2(\vec{p}_1,\vec{r}_2) = \phi_1(\vec{r}_1,\vec{r}_2) + \vec{p}_1\cdot\vec{r}_1, \tag{19a}$$

$$\phi_3(\vec{r}_1,\vec{p}_2) = \phi_1(\vec{r}_1,\vec{r}_2) - \vec{p}_2\cdot\vec{r}_2, \tag{19b}$$

$$\phi_4(\vec{p}_1,\vec{p}_2) = \phi_1(\vec{r}_1,\vec{r}_2) + \vec{p}_1\cdot\vec{r}_1 - \vec{p}_2\cdot\vec{r}_2, \tag{19c}$$

with $\phi_1(\vec{r}_1,\vec{r}_2)$ given by Eq. (2).

It is now of interest to inquire which of the propagator matrix elements is appropriate for the second step of strong-field ionization. Semiclassical scattering characterized by a transition from momentum $\vec{p}_1$ at $t \to -\infty$ to $\vec{p}_2$ at $t \to \infty$ is described by the propagator Eq. (18c) with the compensated action ϕ_4 given by [Eq. (19c)]:

$$\phi_4(\vec{p}_1,\vec{p}_2) = \int_{t_1}^{t_2}\{-\vec{r}(t)\cdot\dot{\vec{p}}(t) - H[\vec{r}(t),\vec{p}(t)]\}dt. \tag{20}$$

For strong-field ionization representing a half-scattering process of an electron initially located near the nucleus and emitted with final momentum $\vec{p}_2(t\to\infty)$, the propagator Eq. (18b) with action ϕ_3 should be applicable for trajectories launched with initial phase $\exp(iI_pt_0)$ according to the time evolution of the ground state. This choice is based on the assumption of well-localized starting points in coordinate space $\vec{r}_1$ near the tunnel exit [Eq. (11)] with negligible phase accumulation under the barrier in position-space representation. We have

$$\phi_3(\vec{r}_1,\vec{p}_2) = \phi_4(\vec{p}_1,\vec{p}_2) - \vec{p}_1\cdot\vec{r}_1. \tag{21}$$

Since in length gauge $\vec{v}_0 = \vec{p}_1$, $\vec{p}_1$ is orthogonal to $\vec{r}_1$ in the limit of vanishing longitudinal velocity at the tunneling exit ($v_{0,z} = 0$) and, hence, ϕ_3 and ϕ_4 coincide. In the following we include the phase contribution $\vec{p}_1\cdot\vec{r}_1$ for nonzero $v_{0,z}$. Its contribution to the interference pattern discussed below is numerically found, however, to be of minor importance.

In our model we restrict ourselves to exponential accuracy. Thus, we ignore the preexponential factor of the matrix element. Using $\phi_3(\vec{r}_1,\vec{p}_2)$ in Eq. (15) yields the semiclassical approximation for the phase corresponding to a given trajectory

$$\begin{aligned}\Phi(t_0^j,\vec{v}_0^j) &= -\vec{v}_0^j\cdot\vec{r}(t_0^j) + I_pt_0^j \\ &\quad - \int_{t_0^j}^{\infty} dt\{\dot{\vec{p}}(t)\cdot\vec{r}(t) + H[\vec{r}(t),\vec{p}(t)]\} \\ &= -\vec{v}_0^j\cdot\vec{r}(t_0^j) + I_pt_0^j - \int_{t_0^j}^{\infty} dt\left\{\frac{p^2(t)}{2} - \frac{2Z}{r(t)}\right\}.\end{aligned} \tag{22}$$

To arrive at this result, $\dot{\vec{p}}$ is expressed in terms of the negative gradient of the total potential containing the electric field and the Coulomb potential. In the case of an arbitrary effective potential $V(\vec{r})$, the Hamiltonian function $H[\vec{r}(t),\vec{p}(t)]$ reads

$$H[\vec{r}(t),\vec{p}(t)] = \frac{p^2(t)}{2} + \vec{F}(t)\cdot\vec{r}(t) + V(\vec{r}) \tag{23}$$

and Newton's equation of motion,

$$\dot{\vec{p}} = -\vec{F}(t) - \vec{\nabla}V[\vec{r}(t)]. \tag{24}$$

Using Eqs. (23) and (24) to derive the integrand in Eq. (20) we obtain from Eq. (21) the following expression for the phase:

$$\begin{aligned}\Phi(t_0^j,\vec{v}_0^j) &= -\vec{v}_0^j\cdot\vec{r}(t_0^j) + I_pt_0^j \\ &\quad - \int_{t_0^j}^{\infty} dt\left\{\frac{p^2(t)}{2} + V[\vec{r}(t)] - \vec{r}(t)\cdot\vec{\nabla}V[\vec{r}(t)]\right\}.\end{aligned} \tag{25}$$

Equation (22) is a special case of Eq. (25) when $V(\vec{r})$ is set to the Coulomb potential $-Z/r$. Equation (25) is applicable to effective one-electron descriptions of ionization of multi-electron systems employing model or pseudopotentials [78]. It should be noted, however, that in the presence of a strong short-ranged contribution to $V(\vec{r})$ the validity of the underlying semiclassical approximation, $\lambda_{dB} \ll R$, where R is the range of the short-ranged contribution, is not obvious and remains to be verified.

For the Coulomb potential $V(\vec{r}) = -Z/r$, the phase of the QTMC model can be obtained from Eq. (25) by omitting the term $\vec{r}(t)\cdot\vec{\nabla}V[\vec{r}(t)]$ in the integrand of Eq. (25). Thus, the semiclassical phase given by Eq. (22) differs from that of the QTMC model [Eq. (17)]: The Coulomb interaction enters with doubled weight. The factor 2 originates from properly accounting for elastic scattering in Eqs. (19b) and (25), i.e., from fully accounting for the Coulomb potential in the compensated action $\phi_4(\vec{p}_1,\vec{p}_2)$. Note, that this compensated action accounts for elastic scattering also in the absence of time-dependent processes. By contrast, Eq. (17) yields for any time-independent Hamiltonian only a trivial trajectory-independent phase $\sim\int dt(H + I_p)$. The QTMC phase can therefore be viewed as an approximation to the full semiclassical phase, Eq. (22).

B. Numerical implementation

In the presence of long-range interactions the calculation of the semiclassical transition amplitude [Eq. (15)] for strong-field ionization requires special care in view of divergent phases and the large number of trajectories for a dense

sampling of phase space needed for achieving sufficient resolution for the multidifferential ionization probability.

We subdivide the integration interval $[t_0^j,\infty]$ into two intervals, $[t_0^j,\tau_f]$ and $[\tau_f,\infty]$, where τ_f is the time at which the laser pulse has concluded and beyond which the energy $H(\tau_f) = E$ is conserved along the outgoing Kepler hyperbola. For pure Coulomb potentials the asymptotic phase-space coordinates $(\vec{k})$ can be determined by the analytic Coulomb mapping of the coordinates $[\vec{r}(\tau_f),\vec{p}(\tau_f)]$ for given energy E,

$$\frac{k^2}{2} = \frac{p^2(\tau_f)}{2} - \frac{1}{r(\tau_f)}, \tag{26}$$

the angular momentum,

$$\vec{L} = \vec{r}(\tau_f) \times \vec{p}(\tau_f), \tag{27}$$

and the Runge-Lenz vector,

$$\vec{a} = \vec{p}(\tau_f) \times \vec{L} - \vec{r}(\tau_f)/r(\tau_f). \tag{28}$$

The asymptotic momentum follows from (see Ref. [39], which corrects the misprint in [79])

$$\vec{k} = k\frac{k(\vec{L}\times\vec{a}) - \vec{a}}{1 + k^2L^2}. \tag{29}$$

The phase Eq. (22) can be analogously decomposed as

$$\Phi\left(t_0^j,\vec{v}_0^j\right) = -\vec{v}_0^j \cdot \vec{r}\left(t_0^j\right) + I_p t_0^j - \int_{t_0^j}^{\tau_f} dt\left\{\frac{p^2(t)}{2} - \frac{2Z}{r(t)}\right\} - \int_{\tau_f}^{\infty} dt\left\{E - \frac{Z}{r(t)}\right\}. \tag{30}$$

We furthermore separate the last term in Eq. (30) representing the scattering phase accumulated in the asymptotic interval $[\tau_f,\infty]$ into the parts with time-independent and time-dependent integrand. The first part yields the linearly divergent contribution

$$\lim_{t\to\infty} E(t - \tau_f). \tag{31}$$

Since only the relative phase between those trajectories arriving in the same bin contribute to the probability (15) whose final momenta and, therefore, energies coincide, the relative phase $(E_j - E_{j'})(t - \tau_f)$ vanishes. This allows for the reduction of the integral for the interval $[\tau_f,\infty]$ to the Coulomb phase,

$$\Phi_f^C(\tau_f) = Z\int_{\tau_f}^{\infty} \frac{dt}{r(t)}, \tag{32}$$

which is still divergent. The regularization of this integral can be performed by analytic Coulomb mapping for Kepler hyperbolae: The distance from the Coulomb center (i.e., from the ion) at a given time t reads (see, e.g., Ref. [80])

$$r(t) = b(g\cosh\xi - 1), \tag{33}$$

where $b = 1/(2E)$, $g = \sqrt{1 + 2EL^2}$, and the parameter $\xi = \xi(t)$ is determined from

$$t = \sqrt{b^3}(g\sinh\xi - \xi) + C. \tag{34}$$

The constant C in Eq. (34) can be found from the initial conditions for the motion in the Coulomb field, i.e., from the position $\vec{r}(\tau_f)$ and momentum $\vec{p}(\tau_f)$ of an electron at $t = \tau_f$. With Eqs. (33) and (34) the integral in Eq. (32) gives

$$\Phi_f^C(\tau_f) = Z\sqrt{b}[\xi(\infty) - \xi(\tau_f)]. \tag{35}$$

Thus, for every trajectory we need to calculate $\xi(\infty)$ and $\xi(\tau_f)$. Since $\xi \to \infty$ for $t \to \infty$, we can discard the decaying exponent in $\sinh\xi = [\exp(\xi) + \exp(-\xi)]/2$ and neglect both C and ξ compared to $\exp(\xi)$ in the asymptotic limit [Eq. (34)]. Consequently, we find for asymptotically large ξ

$$t \approx \sqrt{b^3}g\exp(\xi)/2, \tag{36}$$

from which follows

$$\xi(t\to\infty) \approx \ln\left(\frac{2t}{g\sqrt{b^3}}\right). \tag{37}$$

It is clear that $\xi(t)$ diverges at $t \to \infty$. However, we can isolate the divergent part of Eq. (37), which is common for all the trajectories interfering in a given bin of momentum space, from the finite contributions specific for every individual trajectory. Indeed, we are interested in the relative phases of the interfering trajectories within the same bin, and b depends only on the energy E. Therefore, the common divergent part is given by $\ln(2t/\sqrt{b^3})$, and the finite contribution of every trajectory to the phase [Eq. (30)] is equal to $-\ln(g)$. Note that g depends on both electron energy and angular momentum L. The latter is different for different interfering trajectories within a given bin of the momentum space. For the lower boundary in Eq. (35) we find from Eq. (33)

$$\xi(\tau_f) = \pm\,\mathrm{arcosh}\left\{\frac{1}{g}\left[\frac{r(\tau_f)}{b} + 1\right]\right\}, \tag{38}$$

where the sign still needs to be determined. Taking into account that $dr/dt = \vec{r}\vec{v}/r$ and $dr/dt = (dr/d\xi)/(dt/d\xi)$ and using Eqs. (33) and (34), we find for $\xi(\tau_f)$

$$\xi(\tau_f) = \mathrm{arsinh}\left\{\frac{\vec{r}(\tau_f)\cdot\vec{p}(\tau_f)}{g\sqrt{b}}\right\}. \tag{39}$$

Thus, the finite interference contribution $\tilde{\Phi}_f^C(\tau_f)$ from the Coulomb phase becomes

$$\tilde{\Phi}_f^C(\tau_f) = -Z\sqrt{b}\left[\ln g + \mathrm{arsinh}\left\{\frac{\vec{r}(\tau_f)\cdot\vec{p}(\tau_f)}{g\sqrt{b}}\right\}\right]. \tag{40}$$

We note that such asymptotic Coulomb phase contributions are missing in the QTMC model [53].

In order to achieve convergent semiclassical amplitudes based on Monte-Carlo sampling of a large number of classical trajectories, efficient sampling of initial conditions is essential. One possible method employs initial sets of t_0 and $\vec{v}_0$ that are either uniformly randomly distributed or distributed on a uniform grid (e.g., in Ref. [53]). This results in sampling of a large number of trajectories with relatively small weights [see, e.g., Eq. (9)], which contribute to the final momentum distribution only to a small extent.

Here we implement an alternative Monte Carlo algorithm based on importance sampling. Accordingly, the importance (weight) of a given trajectory is accounted already at the sampling stage, i.e., before the integration of the equations of motion (14). This means that initial sets of t_0 and $\vec{v}_0$ are distributed taking into account the tunneling probability

$w(t_0, v_{0,\perp})$. Importance sampling is a standard method in Monte Carlo integration [81] and is also used in many semiclassical simulations of above-threshold ionization disregarding interference effects (see, e.g., Refs. [22,79]). In the absence of interference effects, the classical probability density $R(\vec{k})$ is calculated within the importance sampling approach as a number of trajectories ending up in a given bin [instead of using Eq. (16) for uniformly distributed initial sets].

Importance sampling is particularly significant in the presence of interference because typically many more trajectories are needed to resolve fine interference structures compared to CTMC simulations without interference (see Sec. IV). Calculation of the ionization probability with trajectories selected by importance sampling is given [instead of Eq. (15)] by

$$R\left(\vec{k}\right) = \left| \sum_{j=1}^{n_p} \exp\left[i\Phi\left(t_0^j, \vec{v}_0^j\right)\right] \right|^2, \tag{41}$$

with ionization times t_0^j and initial velocities $\vec{v}_0^j$ distributed according to the *square root* of the tunneling probability, $\sqrt{w(t_0, \vec{v}_0)}$ [Eq. (9)]. Depending on the laser parameters and tunneling probabilities this importance sampling algorithm can significantly increase the computational speed and convergence as a function of the number of simulated trajectories.

IV. RESULTS AND DISCUSSION

In our simulations we use a few-cycle linearly polarized laser pulse defined in terms of a vector potential that is present between $t = 0$ and $t = \tau_f$,

$$\vec{A}(t) = (-1)^{n+1} \frac{cF_0}{\omega} \sin^2\left(\frac{\omega t}{2n}\right) \sin(\omega t)\vec{e}_z. \tag{42}$$

Here $\vec{e}_z$ is the unit vector pointing in polarization direction and n is the number of optical cycles of the field with $\tau_f = 2\pi n/\omega$. The electric field is obtained from Eq. (42) by $\vec{F}(t) = -\frac{1}{c}\frac{d\vec{A}}{dt}$. We define the vector potential $\vec{A}(t)$ with a prefactor $(-1)^{n+1}$ [Eq. (42)] in order to ensure that the electric field has its maximum at the center of the pulse at $\omega t = \pi n$ for both even and odd numbers of cycles n. We solve Newton's equations of motion using a fourth-order Runge-Kutta method with adaptive step size [81] and calculate the phase [Eq. (22)] by adding an extra equation to the system of equations of motion.

Because of the rotational symmetry with respect to the polarization direction of the laser pulse the semiclassical simulations for a linearly polarized field can be performed employing only two degrees of freedom $(z, r_\perp)$. This reduces the numerical complexity of the problem significantly. Indeed, in order to achieve convergence of the interference oscillations, we need about 1.6×10^9 trajectories (for a comparison, 1.5×10^6 trajectories were sufficient in the CTMC simulation to calculate electron momentum distributions without interference [39]). Nearly the same number of trajectories is used in CCSFA calculations (see, e.g., Ref. [30]). Thus, about 1000 times more trajectories are needed for the semiclassical simulations when interference is included. Simulations of interactions with elliptically or circularly polarized laser fields will require an even larger number of trajectories.

Importance sampling reduces the number of trajectories required to reach convergence of the photoelectron spectrum by a factor 4–5. Typically, we need with importance sampling 4×10^8 trajectories at 800 nm and 1.6×10^9 trajectories at 1200 and 1600 nm. It should be stressed, however, that the performance of numerical approaches employing a uniform distribution of the initial conditions strongly depends on the distribution of initial conditions. The maximum modulus of the initial transverse velocity $v_{0,\perp}$ in the aforementioned example is chosen to correspond to an ionization probability of 10^{-6} of the maximum value of $w(t_0, v_{0,\perp})$ [the latter is achieved for $v_{0,\perp} = 0$; see Eq. (9)] when considering ionization at the field maximum. Moreover, the efficiency depends also on the laser-atom parameters and the calculated observable.

We benchmark our present SCTS model against the exact numerical solution of the time-dependent Schrödinger equation and also compare with results of the previous QTMC model. In order to numerically solve the TDSE

$$i\frac{\partial|\psi(t)\rangle}{\partial t} = \left\{ -\frac{\Delta}{2} + V(r) + zF(t) \right\} |\psi(t)\rangle \tag{43}$$

in the dipole approximation for a single active electron, we employ the generalized pseudospectral method [82–84]. This method combines the discretization of the radial coordinate optimized for the Coulomb singularity with quadrature methods to allow stable long-time evolution using a split-operator representation of the time-evolution operator. Both the bound as well as the unbound parts of the wave function $|\psi(t)\rangle$ can be accurately represented. The atomic potential $V(r)$ is taken to be the Coulomb potential, $V(r) = -1/r$. Propagation of the wave function is started from the ground state of hydrogen. Due to the cylindrical symmetry of the system, the magnetic quantum number $m = 0$ is conserved. After the end of the laser pulse the wave function is projected on eigenstates $|k, \ell\rangle$ of the free atomic Hamiltonian with positive eigenenergy $E = k^2/2$ and orbital quantum number ℓ to determine the transition probabilities $R(\vec{k})$ to reach the final state $|\phi_{\vec{k}}\rangle$ (see Refs. [85–87]):

$$R(\vec{k}) = \frac{1}{4\pi k} \left| \sum_l e^{i\delta_\ell(k)} \sqrt{2l+1} P_\ell(\cos\theta) \langle k, \ell|\psi(t_f)\rangle \right|^2. \tag{44}$$

In Eq. (44), $\delta_\ell(k)$ is the momentum-dependent atomic phase shift, θ is the angle between the electron momentum $\vec{k}$ and the polarization direction of the laser field $\vec{e}_z$ and P_ℓ is the Legendre polynomial of degree ℓ. In order to avoid unphysical reflections of the wave function at the boundary of the system, the length of the computing box was chosen to be 1200 a.u. (~65 nm), which is much larger than the maximum quiver amplitude $\alpha = F_0/\omega^2 = 62$ a.u. at the intensity of 0.9×10^{14} W/cm^2 and the wavelength of 1600 nm. The maximum angular momentum included was $\ell_{\max} = 300$.

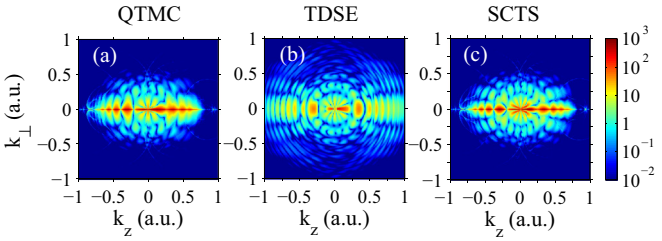

FIG. 1. Vectorial momentum distributions for the H atom ionized by a laser pulse with a duration of $n = 8$ cycles, wavelength of $\lambda = 800$ nm, and peak intensity of $I = 0.9 \times 10^{14}$ W/cm^2 obtained from (a) the QTMC model, (b) solution of the TDSE, and (c) the present SCTS model. The distributions are normalized to the total ionization yield. A logarithmic color scale in arbitrary units is used. The laser field is linearly polarized along the z axis.

We first turn our attention to the vectorial photoelectron momentum distribution in the $(k_z,k_\perp)$ plane (Fig. 1). For the semiclassical simulations we first employ the initial distribution [Eq. (9)] with zero initial parallel velocity. Important features of the TDSE momentum distribution are reproduced by both the SCTS and the QTMC models: The distributions are stretched along the polarization axis with clear ATI rings and a central interference structure at small momenta. The spread of the distribution along the polarization axis is underestimated by both semiclassical models due to the initial condition $v_{0,z} = 0$ (see below).

A close-up of the low-energy spectrum (Fig. 2) shows marked differences between the different models. For $|k| \leqslant 0.3$ a.u. and energies well below $U_p = 0.2$ a.u., the vectorial momentum distribution displays a fanlike interference structure similar to that of Ramsauer-Townsend diffraction oscillations [50,51,88,89]. The number of radial nodal lines is controlled by the dominant partial-wave angular momentum ℓ_c in Eq. (44); i.e., $R(\vec{k}) \sim |P_{l_c}(\cos\theta)|^2$ (see Refs. [88,89]). While the SCTS model closely matches the nodal pattern of the TDSE, the QTMC model yields fewer nodal lines, which is a direct consequence of the underestimate of the Coulomb interaction in the QTMC treatment of the interference phase. This effect of neglecting the elastic scattering in the Coulomb field occurs both during the laser pulse [Eq. (30)] and after [Eq. (40)]. The magnitude of the latter is illustrated in Fig. 3 where we display the effect of $\tilde{\Phi}_f^C(\tau_f)$ for both an ultrashort single-cycle pulse and the longer eight-cycle pulse. The postpulse Coulomb phase is more pronounced for shorter τ_f as the electron is still closer to the nucleus at the end of the pulse.

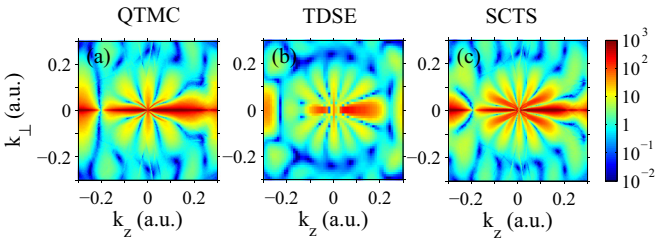

FIG. 2. Magnification of Fig. 1 for $|k_z|,|k_\perp| < 0.3$ a.u.

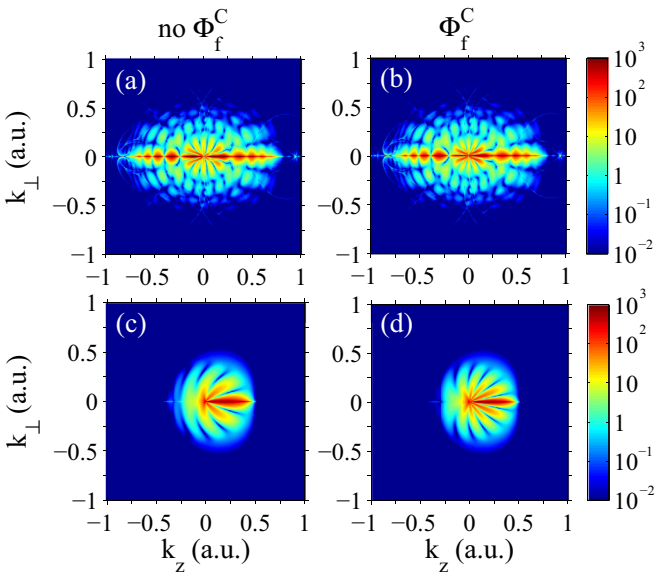

FIG. 3. Vectorial momentum distribution from the present SCTS model for low-energy electrons without (a),(c) and with (b),(d) inclusion of the postpulse Coulomb phase $\tilde{\Phi}_f^C(\tau_f)$ [Eq. (40)] for the eight-cycle pulse of Fig. 1 (a),(b) and a single-cycle pulse (c),(d) with all other laser parameters identical. The distributions are normalized to the total ionization yield. A logarithmic color scale in arbitrary units is used.

For a quantitative comparison of different methods we consider the singly differential angular distribution (Fig. 4)

$$\frac{dR}{\sin\theta d\theta} = 2\pi \int_0^\infty dE\sqrt{2E}\,R[\vec{k}(E)] \tag{45}$$

and the photoelectron spectrum

$$\frac{dR}{dE} = 2\pi\sqrt{2E}\int_0^\pi d\theta \sin\theta\, R[\vec{k}(\theta)]. \tag{46}$$

The energy spectra feature pronounced ATI peaks. These are qualitatively reproduced by the semiclassical methods. However, only for the low-order peaks can the semiclassical approximation quantitatively reproduce the amplitude of the oscillations [52]. This is closely related to the fact that the initial conditions from the tunneling step [Eq. (9)] provide too few trajectories with large longitudinal momenta that could account for intercycle interferences, the semiclassical origin of the ATI modulation at large momenta. For the same reason the photoelectron spectrum dR/dE falls off too rapidly for energies exceeding $\sim U_p$. The semiclassical angular distributions reproduce the Ramsauer-Townsend diffraction oscillations [88,89]. The modulation amplitude as well as the position of the minima of the SCTS agree better with the TDSE compared to the QTMC model because of the improved interference phase. The difference is more pronounced for the angular distribution of low-energy electrons (Fig. 5).

Obviously, further improvement of the semiclassical description of the energy and angular distributions of photoelectrons require an improved initial distribution emerging from the tunneling step. To this end, we set the initial conditions for the propagation of classical trajectories, we

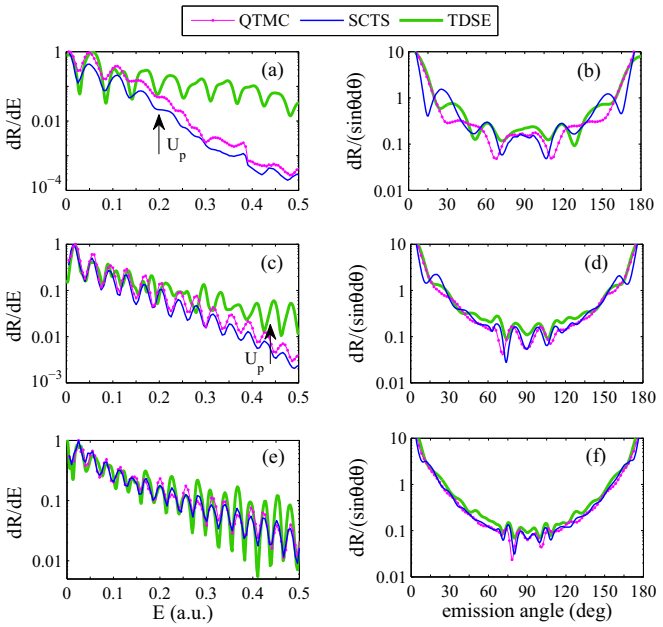

FIG. 4. Energy spectra (a),(c),(e) and angular distributions (b),(d),(f) of the photoelectrons for ionization of H at an intensity of 9×10^{13} W/cm^2 and a pulse duration of eight cycles obtained from the QTMC model [thin (magenta) curve with solid circles], the SCTS model [solid (blue) curve], and TDSE [thick (green) curve]. The distributions [(a),(b)], [(c),(d)], and [(e),(f)] correspond to the wavelengths of 800, 1200, and 1600 nm, with Keldysh parameters of 1.12, 0.75, and 0.56, respectively. The energy spectra are normalized to the peak value; the angular distributions are normalized to the total ionization yield and show the spectrum for electrons with asymptotic energies $E < U_p$. The energy equal to U_p is shown by arrows in panels (a) and (c).

set the initial parallel velocity $v_{0,z}$ at every ionization time t_0 in Eq. (9) to a nonzero value predicted by the strong-field approximation (see Refs. [30,58,59,71]). For the pulse defined in Eq. (42) it can be, for a sufficiently long pulse, approximated by

$$v_{z,0}(t_0) = -\frac{1}{c} A_z(t_0)[\sqrt{1+\gamma^2(t_0, v_{0,\perp})} - 1], \qquad (47)$$

where

$$\gamma(t_0, v_{0,\perp}) = \frac{\omega\sqrt{2I_p + v_{0,\perp}^2}}{F_0 \sin^2\left(\frac{\omega t_0}{2n}\right)|\cos(\omega t_0)|} \qquad (48)$$

is the effective Keldysh parameter [71]. In the tunneling limit $\gamma(t_0, v_{0,\perp}) \to 0$ the longitudinal initial velocity $v_{z,0}(t_0)$ vanishes.

Employing Eq. (47) as initial condition for CTMC trajectories taking off at t_0 at the tunneling exit yields improved agreement between the SCTS model and the TDSE for both the vectorial momentum distribution (Fig. 6) and the singly differential distributions dR/dE and $dR/(\sin\theta d\theta)$ (Fig. 7).

Indeed, the SCTS model can now better reproduce the energy spectrum obtained from the TDSE; see Fig. 7(a). For angular distribution the agreement between the QTMC and the TDSE worsens, whereas the agreement between the SCTS and the TDSE improves [compare Fig. 7(b) with Fig. 4(b)]. These

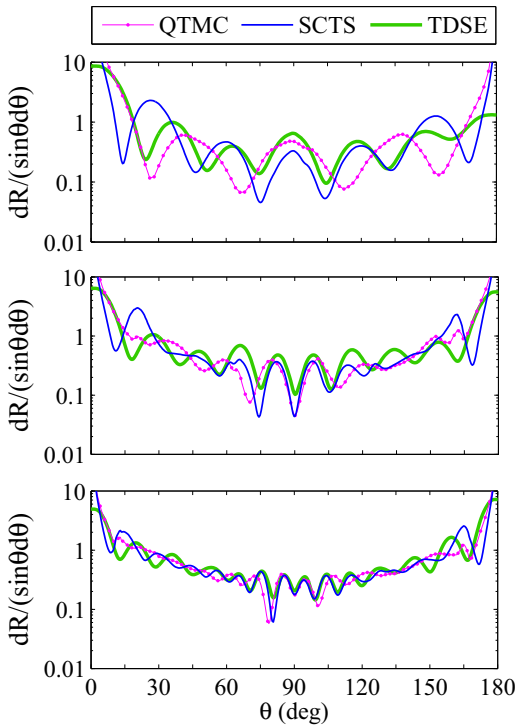

FIG. 5. Angular distributions for low-energy electrons (innermost fanlike structure; cf. Fig. 2): (a) $E < 0.022$ a.u. for $\lambda = 800$ nm, (b) $E < 0.031$ a.u. for $\lambda = 1200$ nm, and (c) $E < 0.036$ a.u. for $\lambda = 1600$ nm. Cutoff energies have been determined from TDSE results.

results clearly suggest that the main source of deviations of the SCTS model from the TDSE are the errors in treating the tunneling step rather than the semiclassical description of the post-tunneling propagation.

V. CONCLUSIONS AND OUTLOOK

We have developed a semiclassical two-step model for strong-field ionization that describes quantum interference and accounts for the Coulomb potential beyond the semiclassical perturbation theory. In the SCTS model the phase associated with every classical trajectory is calculated using the semiclassical expression for the matrix element of the quantum mechanical propagator. For identical initial conditions after

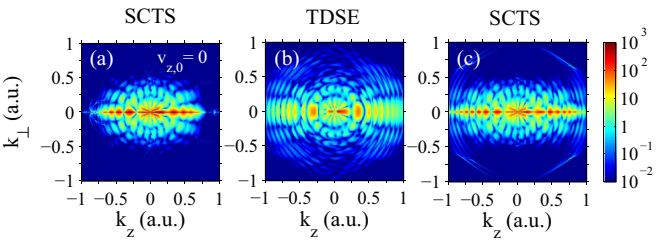

FIG. 6. Vectorial momentum distributions obtained from (a) SCTS model with zero initial parallel velocity, (b) solution of the TDSE, and (c) the SCTS model with nonzero initial parallel velocity. The parameters are the same as in Fig. 1. Panel (a) is the same as Fig. 1(c). A logarithmic color scale in arbitrary units is used.

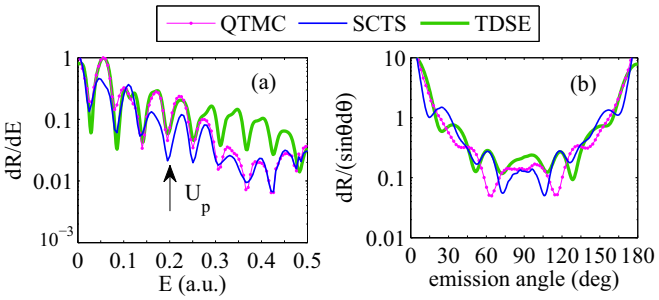

FIG. 7. Same as Fig. 4 for $\lambda = 800$ nm with nonzero initial parallel velocity.

the tunneling ionization step taken from standard tunnel ionization rates [1], the SCTS model yields closer agreement with the exact solution of the Schrödinger equation than the previously proposed QTMC model. Furthermore, after improving the input from the tunneling ionization step by including nonzero parallel velocities in the initial conditions for the motion after tunneling, the SCTS model yields significantly improved agreement in the angular distribution, i.e., the position of interference fringes with the TDSE results. Remaining differences in the intensity of energy distributions are traced back to improvable starting conditions (in particular the choice of parallel velocities) of classical trajectories.

The present SCTS model can be extended to multielectron targets in a straightforward fashion by the inclusion of dynamical Stark shifts and polarization-induced dipole potentials. To this end, the SCTS model can be combined with the semiclassical approach developed in Refs. [37,39] that is based on the effective potential for the outer electron [75]. This effective potential includes the laser field, the Coulomb field, and the polarization effects of the inner core. Semiclassical models of this type will make it possible to investigate the role of the multielectron polarization effect in the formation of the interference structure in the electron momentum distributions. Since the multielectron potential affects both the exit point and the electron dynamics in the continuum, pronounced imprints of the polarization effects in the interference patterns are expected. Finally, the two-step semiclassical models accounting for both the interference and the multielectron effects can provide a valuable tool for investigation of the delays in photoemission, which is presently one of the most intensively studied problems in strong-field physics and attosecond science.

ACKNOWLEDGMENTS

We are grateful to Janne Solanpää (Tampere University of Technology) for stimulating discussions. This work has been supported by the European Community's FP7 through CRONOS Project No. 280879, Academy of Finland Project No. 267686, Nordic Innovation through Top-Level Research Initiative Project No. P-13053, COST Action No. CM-1204 (XLIC-XUV/x-ray light and fast ions for ultrafast chemistry), the STSM Grant from COST Action No. CM-1204, an ERC-StG (Project No. 277767, TDMET), the VKR Center of Excellence QUSCOPE, FWF-SFB049 NextLite, CONICET (Argentina Grant No. PIP0386), ANPCyT (Argentina Grant No. PICT-2014-2363), and UBACyT0617BA.

[1] N. B. Delone and V. P. Krainov, *Multiphoton Processes in Atoms* (Springer, Berlin, 2000), Chap. 9.

[2] W. Becker, F. Grasbon, R. Kopold, D. B. Milošević, G. G. Paulus, and H. Walther, Above-threshold ionization: from classical features to quantum effects, Adv. At. Mol. Opt. Phys. **48**, 35 (2002).

[3] D. B. Milošević and F. Ehlotzky, Scattering and reaction processes in powerful laser fields, Adv. At. Mol. Opt. Phys. **49**, 373 (2003).

[4] A. Becker and F. H. M. Faisal, Intense-field many-body S-matrix theory, J. Phys. B: At. Mol. Opt. Phys. **38**, R1 (2005).

[5] C. Figueira de Morisson Faria and X. Liu, Electron-electron correlation in strong laser fields, J. Mod. Opt. **58**, 1076 (2011).

[6] L. V. Keldysh, Ionization in the field of a strong electromagnetic wave, Zh. Eksp. Teor. Fiz. **47**, 1945 (1964) [Sov. Phys. JETP **20**, 1307 (1965)].

[7] F. H. M. Faisal, Multiple absorption of laser photons by atoms, J. Phys. B.: At. Mol. Opt. Phys. **6**, L89 (1973).

[8] H. R. Reiss, Effect of an intense electromagnetic field on a weakly bound system, Phys. Rev. A **22**, 1786 (1980).

[9] L. D. Landau and E. M. Lifshitz, *Quantum Mechanics Non-relativistic Theory*, 2nd ed. (Pergamon, Oxford, U.K., 1965).

[10] A. M. Perelomov, V. S. Popov, and M. V. Terent'ev, Ionization of atoms in an alternating electric field, Zh. Eksp. Teor. Fiz. **50**, 1393 (1966) [Sov. Phys. JETP **23**, 924 (1966)].

[11] M. V. Ammosov, N. B. Delone, and V. P. Krainov, Tunnel ionization of complex atoms and of atomic ions in an alternating electromagnetic field, Zh. Eksp. Teor. Fiz. **91**, 2008 (1986) [Sov. Phys. JETP **64**, 1191 (1986)].

[12] H. B. van Linden van den Heuvell and H. G. Muller, in *Multiphoton Processes*, edited by S. J. Smith and P. L. Knight (Cambrige University Press, Cambrige, U.K., 1988).

[13] T. F. Gallagher, Above-Threshold Ionization in Low-Frequency Limit, Phys. Rev. Lett. **61**, 2304 (1988).

[14] P. B. Corkum, N. H. Burnett, and F. Brunel, Above-Threshold Ionization in the Long-Wavelength Limit, Phys. Rev. Lett. **62**, 1259 (1989).

[15] K. C. Kulander, K. J. Schafer, and J. L. Krause, in *Super-Intense Laser-Atom Physics*, edited by B. Pireaux, A. L'Hullier, and K. Rzazewski (Plenum, New York, 1993).

[16] P. B. Corkum, Plasma Perspective on Strong Field Multiphoton Ionization, Phys. Rev. Lett. **71**, 1994 (1993).

[17] H. G. Muller, An efficient propagation scheme for the time-dependent Schrödinger equation in the velocity gauge, Laser Phys. **9**, 138 (1999).

[18] D. Bauer and P. Koval, Qprop: A Schrödinger-solver for intense laseratom interaction, Comput. Phys. Commun. **174**, 396 (2006).

[19] J. L. Krause, K. J. Schafer, and K. C. Kulander, High-Order Harmonic Generation from Atoms and Ions in the High Intensity Regime, Phys. Rev. Lett. **68**, 3535 (1992).

[20] M. Lewenstein, Ph. Balcou, M. Yu. Ivanov, A. L'Huillier, and P. B. Corkum, Theory of high-harmonic generation by low-frequency laser fields, Phys. Rev. A **49**, 2117 (1994).

[21] G. G. Paulus, W. Nicklich, H. Xu, P. Lambropoulos, and H. Walther, Plateau in Above Threshold Ionization Spectra, Phys. Rev. Lett. **72**, 2851 (1994).

[22] G. G. Paulus, W. Becker, W. Nicklich, and H. Walther, Rescattering effects in above-threshold ionization: A classical model, J. Phys. B **27**, L703 (1994).

[23] C. Figueira de Morisson Faria and W. Becker, Quantum-orbit analysis of nonsequential double ionization, Laser Phys. **13**, 1196 (2003).

[24] D. B. Milošević and W. Becker, Classical cutoffs for laser-induced nonsequential double ionization, Phys. Rev. A **68**, 065401 (2003).

[25] T. Brabec, M. Yu. Ivanov, and P. B. Corkum, Coulomb focusing in intense field atomic processes, Phys. Rev. A **54**, R2551(R) (1996).

[26] K. Dimitriou, D. G. Arbó, S. Yoshida, E. Persson, and J. Burgdörfer, Origin of the double-peak structure in the momentum distribution of ionization of hydrogen atoms driven by strong laser fields, Phys. Rev. A **70**, 061401(R) (2004).

[27] C. I. Blaga, F. Catoire, P. Colosimo, G. G. Paulus, H. G. Muller, P. Agostini, and L. F. DiMauro, Strong-field photoionization revisited, Nat. Phys. **5**, 335 (2009).

[28] W. Quan, Z. Lin, M. Wu, H. Kang, H. Liu, X. Liu, J. Chen, J. Liu, X. T. He, S. G. Chen *et al.*, Classical Aspects in Above-Threshold Ionization with a Midinfrared Strong Laser Field, Phys. Rev. Lett. **103**, 093001 (2009).

[29] C. Liu and K. Z. Hatsagortsyan, Origin of Unexpected Low Energy Structure in Photoelectron Spectra Induced by Midinfrared Strong Laser Fields, Phys. Rev. Lett. **105**, 113003 (2010).

[30] T.-M. Yan, S. V. Popruzhenko, M. J. J. Vrakking, and D. Bauer, Low-Energy Structures in Strong Field Ionization Revealed by Quantum Orbits, Phys. Rev. Lett. **105**, 253002 (2010).

[31] A. Kästner, U. Saalmann, and J. M. Rost, Electron-Energy Bunching in Laser-Driven Soft Recollisions, Phys. Rev. Lett. **108**, 033201 (2012).

[32] C. Lemell, K. I. Dimitriou, X. M. Tong, S. Nagele, D. V. Kartashov, J. Burgdörfer, and S. Gräfe, Low-energy peak structure in strong-field ionization by midinfrared laser pulses: Two-dimensional focusing by the atomic potential, Phys. Rev. A **85**, 011403(R) (2012).

[33] C. Lemell, J. Burgdörfer, K. I. Dimitriou, D. G. Arbó, and X.-M. Tong, Classical-quantum correspondence in atomic ionization by midinfrared pulses: Multiple peak and interference structures, Phys. Rev. A **87**, 013421 (2013).

[34] B. Wolter, C. Lemell, M. Baudish, M. G. Pullen, X.-M. Tong, M. Hemmer, A. Senftleben, C. D. Schröter, J. Ullrich, R. Moshammer, J. Biegert, and J. Burgdörfer, Formation of very-low-energy states crossing the ionization threshold of argon atoms in strong mid-infrared fields, Phys. Rev. A **90**, 063424 (2014).

[35] W. Becker, S. P. Goreslavski, D. B. Milošević, and G. G. Paulus, Low-energy electron rescattering in laser-induced ionization, J. Phys. B: At. Mol. Opt. Phys. **47**, 204022 (2014).

[36] D. Dimitrovski and L. B. Madsen, Theory of low-energy photoelectrons in strong-field ionization by laser pulses with large ellipticity, Phys. Rev. A **91**, 033409 (2015).

[37] A. N. Pfeiffer, C. Cirelli, M. Smolarski, D. Dimitrovski, M. Abu-Samha, L. B. Madsen, and U. Keller, Attoclock reveals geometry for laser-induced tunneling, Nat. Phys. **8**, 76 (2012).

[38] J. Maurer, D. Dimitrovski, L. Christensen, L. B. Madsen, and H. Stapelfeldt, Molecular-Frame 3D Photoelectron Momentum Distributions by Tomographic Reconstruction, Phys. Rev. Lett. **109**, 123001 (2012).

[39] N. I. Shvetsov-Shilovski, D. Dimitrovski, and L. B. Madsen, Ionization in elliptically polarized pulses: Multielectron polarization effects and asymmetry of photoelectron momentum distributions, Phys. Rev. A **85**, 023428 (2012).

[40] R. Boge, C. Cirelli, A. S. Landsman, S. Heuser, A. Ludwig, J. Maurer, M. Weger, L. Gallmann, and U. Keller, Probing Nonadiabatic Effects in Strong-Field Tunnel Ionization, Phys. Rev. Lett. **111**, 103003 (2013).

[41] C. Hofmann, A. S. Landsman, A. Zielinski, C. Cirelli, T. Zimmermann, A. Scrinzi, and U. Keller, Interpreting electron-momentum distributions and nonadiabaticity in strong-field ionization, Phys. Rev. A **90**, 043406 (2014).

[42] J.-W. Geng, L. Qin, M. Li, W.-H. Xiong, Y. Liu, Q. Gong, and L.-Y. Peng, Nonadiabatic tunneling ionization of atoms in elliptically polarized laser fields, J. Phys. B: At. Mol. Opt. Phys. **47**, 204027 (2014).

[43] N. I. Shvetsov-Shilovski, S. P. Goreslavski, S. V. Popruzhenko, and W. Becker, Ellipticity effects and the contributions of long orbits in nonsequential double ionization of atoms, Phys. Rev. A **77**, 063405 (2008).

[44] X. Wang and J. H. Eberly, Effects of Elliptical Polarization on Strong-Field Short-Pulse Double Ionization, Phys. Rev. Lett. **103**, 103007 (2009).

[45] X. L. Hao, G. Q. Wang, X. Y. Jia, W. D. Li, J. Liu, and J. Chen, Nonsequential double ionization of Ne in an elliptically polarized intense laser field, Phys. Rev. A **80**, 023408 (2009).

[46] F. Mauger, C. Chandre, and T. Uzer, Recollisions and Correlated Double Ionization with Circularly Polarized Light, Phys. Rev. Lett. **105**, 083002 (2010).

[47] A. Emmanouilidou and D. S. Tchitchekova, Strongly driven molecules: Traces of soft recollisions for intermediate intensities in the over-the-barrier regime, Phys. Rev. A **84**, 033407 (2011).

[48] N. I. Shvetsov-Shilovski, D. Dimitrovski, and L. B. Madsen, Ehrenfest's theorem and the validity of the two-step model for strong-field ionization, Phys. Rev. A **87**, 013427 (2013).

[49] Ph. A. Korneev, S. V. Popruzhenko, S. P. Goreslavski, T.-M. Yan, D. Bauer, W. Becker, M. Kübel, M. F. Kling, C. Rödel, and G. G. Paulus, Interference Carpets in Above-Threshold Ionization: From the Coulomb-Free to the Coulomb-Dominated Regime, Phys. Rev. Lett. **108**, 223601 (2012).

[50] D. G Arbó, E. Persson, and J. Burgdörfer, Time double-slit interferences in strong-field tunneling ionization, Phys. Rev. A **74**, 063407 (2006).

[51] R. Gopal, K. Simeonidis, R. Moshammer, Th. Ergler, M. Dürr, M. Kurka, K.-U. Kühnel, S. Tschuch, C.-D. Schröter, D. Bauer, and J. Ullrich, Three-Dimensional Momentum Imaging of Electron Wave Packet Interference in Few-Cycle Laser Pulses, Phys. Rev. Lett. **103**, 053001 (2009).

[52] D. G Arbó, K. L. Ishikawa, K. Schiessl, E. Persson, and J. Burgdörfer, Intracycle and intercycle interferences in above-threshold ionization: The time grating, Phys. Rev. A **81**, 021403(R) (2010).

[53] M. Li, J.-W. Geng, H. Liu, Y. Deng, C. Wu, L.-Y. Peng, Q. Gong, and Y. Liu, Classical-Quantum Correspondence for Above-Threshold Ionization, Phys. Rev. Lett. **112**, 113002 (2014).

[54] T. Minami, C. O. Reinhold, and J. Burgdörfer, Quantum-trajectory Monte Carlo method for internal-state evolution of fast ions traversing amorphous solids, Phys. Rev. A **67**, 022902 (2003).

[55] M. Li, X. Sun, X. Xie, Y. Shao, Y. Deng, C. Wu, Q. Gong, and Y. Liu, Revealing backward rescattering photoelectron interference of molecules in strong infrared laser fields, Sci. Rep. **5**, 8519 (2015).

[56] Y. Shao, M.-M. Liu, X. Sun, X. Xie, P. Wang, Y. Deng, C. Wu, Q. Gong, and Y. Liu, Isolating resonant excitation from above-threshold ionization, Phys. Rev. A **92**, 013415 (2015).

[57] J.-W. Geng, W.-H. Xiong, X.-R. Xiao, L.-Y. Peng, and Q. Gong, Nonadiabatic Electron Dynamics in Orthogonal Two-Color Laser Fields with Comparable Intensities, Phys. Rev. Lett. **115**, 193001 (2015).

[58] S. V. Popruzhenko and D. Bauer, Strong field approximation for systems with Coulomb interaction, J. Mod. Opt. **55**, 2573 (2008).

[59] S. V. Popruzhenko, G. G. Paulus, and D. Bauer, Coulomb-corrected quantum trajectories in strong-field ionization, Phys. Rev. A **77**, 053409 (2008).

[60] A. M. Perelomov and V. S. Popov, Ionization of atoms in an alternating electrical field III, Zh. Eksp. Teor. Fiz. **52**, 514 (1967) [Sov. Phys. JETP **25**, 336 (1967)].

[61] D. J. Tannor, *Introduction to Quantum Mechanics: A Time-Dependent Perspective* (University Science Books, Sausalito, California, 2007).

[62] F. Grossmann, *Theoretical Femtosecond Physics. Atoms and Molecules in Srong Laser Fields* (Springer-Verlag, Berlin, Heidelberg, 2008).

[63] W. H. Miller, Classical-limit quantum mechanics and the theory of molecular collisions, Adv. Chem. Phys. **25**, 69 (1971).

[64] M. Walser and T. Brabec, Semiclassical path integral theory of strong-laser-field physics, J. Phys. B **36**, 3025 (2003).

[65] M. Spanner, Strong Field Tunnel Ionization by Real-Valued Classical Trajectories, Phys. Rev. Lett. **90**, 233005 (2003).

[66] S. Yoshida, F. Grossmann, E. Persson, and J. Burgdörfer, Semiclassical analysis of quantum localization of the periodically kicked Rydberg atom, Phys. Rev. A **69**, 043410 (2004).

[67] D. B. Milošević, G. G. Paulus, D. Bauer, and W. Becker, Above-threshold ionization by few-cycle pulses, J. Phys. B **39**, R203 (2006).

[68] T. Yan and D. Bauer, Sub-barrier Coulomb effects on the interference pattern in tunneling-ionization photoelectron spectra, Phys. Rev. A **86**, 053403 (2012).

[69] P. Salières, B. Carré, L. Le Déroff, F. Grasbon, G. G. Paulus, H. Walther, R. Kopold, W. Becker, D. B. Milošević, A. Sanpera, and M. Lewenstein, Feynman's path-integral approach for intense-laser-atom interactions, Science **292**, 902 (2001).

[70] G. L. Yudin and M. Yu. Ivanov, Nonadiabatic tunnel ionization: Looking inside a laser cycle, Phys. Rev. A **64**, 013409 (2001).

[71] M. Li, J.-W. Geng, M. Han, M.-M. Liu, L.-Y. Peng, Q. Gong, and Y. Liu, Subcycle nonadiabatic strong-field tunneling ionization, Phys. Rev. A **93**, 013402 (2016).

[72] M. Born, *Vorlesungen über Atommechanik* (Springer, Berlin, 1925), p. 243.

[73] E. Schrödinger, Ann. Phys. (Berlin, Ger.) **385**, 437 (1926).

[74] C. Z. Bisgaard and L. B. Madsen, Tunneling ionization of atoms, Am. J. Phys. **72**, 249 (2004).

[75] D. Dimitrovski, C. P. J. Martiny, and L. B. Madsen, Strong-field ionization of polar molecules: Stark-shift-corrected strong-field approximation, Phys. Rev. A **82**, 053404 (2010).

[76] C. Reinhold, S. Yoshida, J. Burgdörfer, B. Wyker, J. Mestayer, and F. Dunning, Large-scale quantum coherence of nearly circular wave packets, J. Phys. B **42**, 091003 (2009).

[77] K. G. Kay, Semiclassical initial value treatments of atoms and molecules, Annu. Rev. Phys. Chem. **56**, 255 (2005).

[78] X.-M. Tong, G. Wachter, S. Sato, C. Lemell, K. Yabana, and J. Burgdörfer, Application of norm-conserving pseudopotentials to intense laser-matter interactions, Phys. Rev. A **92**, 043422 (2015), and references therein.

[79] N. I. Shvetsov-Shilovski, S. P. Goreslavski, S. V. Popruzhenko, and W. Becker, Capture into Rydberg states and momentum distributions of ionized electrons, Laser Phys. **19**, 1550 (2009).

[80] L. D. Landau and E. M. Lifshitz, *Mechanics*, 2nd ed. (Pergamon, Oxford, U.K., 1969).

[81] W. H. Press, S. A. Teukolsky, W. T. Vetterling, and B. P. Flannery, *Numerical Recipes in Fortran 77: The Art of Scientific Computing*, 2nd ed. (Cambridge University Press, Cambridge, U.K., 1992).

[82] X.-M. Tong and S. I. Chu, Theoretical study of multiple high-order harmonic generation by intense ultrashort pulsed laser fields: A new generalized pseudospectral time-dependent method, Chem. Phys. **217**, 119 (1997).

[83] X.-M. Tong and S.-I Chu, Time-dependent approach to high-resolution spectroscopy and quantum dynamics of Rydberg atoms in crossed magnetic and electric fields, Phys. Rev. A **61**, 031401(R) (2000).

[84] X.-M. Tong and C. D. Lin, Empirical formula for static field ionization rates of atoms and molecules by lasers in the barrier-suppression regime, J. Phys. B **38**, 2593 (2005).

[85] O. Schöller, J. S. Briggs, and R. M. Dreizler, Coherent excitation of hydrogen atoms by proton impact, J. Phys. B **19**, 2505 (1986).

[86] A. Messiah, *Quantum Mechanics 1* (North-Holland, New York, 1965).

[87] S. Dionissopoulou, Th. Mercouris, A. Lyras, and C. A. Nicolaides, Strong laser-field effects in hydrogen: High-order above-threshold ionization and photoelectron angular distributions, Phys. Rev. A **55**, 4397 (1997).

[88] D. G Arbó, S. Yoshida, E. Persson, K. I. Dimitriou, and J. Burgdörfer, Interference Oscillations in the Angular Distribution of Laser-Ionized Electrons Near Ionization Threshold, Phys. Rev. Lett. **96**, 143003 (2006).

[89] D. G Arbó, E. Persson, K. I. Dimitriou, and J. Burgdörfer, Sub-Poissonian angular momentum distribution near threshold in atomic ionization by short laser pulses, Phys. Rev. A **78**, 013406 (2008).